

VIBRATIONAL SPECTRA AND THE STRUCTURE OF THE $(1-x)\text{Li}_{0.42}\text{K}_{0.58}\text{NO}_3 - x\text{Al}_2\text{O}_3$ SYSTEM

M. M. Gafurov^{1,2}, K. Sh. Rabadanov¹,
A. M. Amirov¹, M. B. Ataev¹, Z. Yu. Kubataev¹,
and M. G. Kakagasanov^{1,2}

Vibrational spectroscopy and X-ray diffraction are used to study phase compositions and structural properties of composite systems (composites) based on the $\text{LiNO}_3-\text{KNO}_3$ eutectic binary system with the addition of alumina nanopowder. High nanopowder concentrations are shown to cause amorphization of the salt system.

DOI: 10.1134/S0022476619030089

Keywords: composite, binary system, lithium nitrate, potassium nitrate, Raman scattering, infrared absorption, powder X-ray diffraction.

INTRODUCTION

Despite the progress in the synthesis of novel solid electrolytes with alkali metal cation conductivity, most solid ionic conductors have shortcomings to hinder their practical application. The most common of them are insufficiently high electrical conductivity, especially at ambient temperatures, chemical interaction with electrode materials and the atmosphere, low decomposition potential, poor ceramic properties, insufficient heat resistance. Therefore, further studies aimed at synthesizing new solid electrolytes and improving the characteristics of currently available electrolytes are still an urgent task. Composite solid electrolytes based on alkali metal salts and oxide powders exhibit higher electrical conductivity than original salts [1-3]. This circumstance causes increased interest to the studies of such systems primarily because no unequivocal answer has yet been given to the question of why ionic conductivity of composites is increased substantially by simple mixing of two dielectrics (oxide + ionic salt). Also, the use of multicomponent salt systems (eutectics) allows obtaining relatively low temperature electrolytes. At the same time, this circumstance opens up broad technological prospects for the synthesis of new composite systems by using ionic salts and oxides of various compositions, size, production conditions, etc. [4, 5]. The data reported to date concern mainly the studies of electrophysical properties [1, 6]. Obviously, the microstructure, dynamic interactions of ions, molecules, and nanoparticles are to be studied in more detail to understand the reasons and the mechanisms underlying the increase of ionic conductivity. Therefore, studying composites of various phase and aggregate states using spectroscopic [7, 8], X-ray diffraction [9], thermophysical [10], and other methods [11] to obtain complete data about their structure and elementary dynamic processes will make it possible to identify the mechanisms of ionic conductivity and optimize the synthesis pathways of new solid-state electrolyte systems of complex compositions.

¹Analytical Center of Joint Usage, Dagestan Scientific Center, Russian Academy of Sciences, Makhachkala, Russia; rksh83@mail.ru. ²Amirkhanov Institute of Physics, Dagestan Scientific Center, Russian Academy of Sciences, Makhachkala, Russia. Translated from *Zhurnal Strukturnoi Khimii*, Vol. 60, No. 3, pp. 422-429, March, 2019. Original article submitted April 09, 2018; revised September 24, 2018; accepted November 01, 2018.

In this work, vibrational spectroscopy and X-ray diffraction methods are used to study the effect of the nanosized (nanocrystalline) Al_2O_3 filler on the structure of the eutectic (binary) $\text{LiNO}_3\text{--KNO}_3$ mixture.

EXPERIMENTAL

The composite system was obtained using the following reagents: lithium nitrate (analytical-grade, "Ekros"), potassium nitrate (reagent-grade, "Ekros"), $\gamma\text{-Al}_2\text{O}_3$ (99%, "ABCR") with specific surface of $120 \text{ m}^2/\text{g}$ and the average particle size of 15–20 nm. Lithium nitrate was dried in a vacuum using a backing vacuum pump at 150°C for at least 24 h.

The eutectic salt system chosen for the study was $0.42\text{LiNO}_3\text{--}0.58\text{KNO}_3$ (in molar fractions). The alumina powder for the surface dehydration was preliminary calcinated for 2 h at 500°C . The composites were prepared by heating the eutectic mixture and the oxide at 250°C and then mixing them thoroughly in an inert atmosphere. After cooling, the resulting composite was ground in an agate mortar and sealed in pyrex tubes. All the work was carried out in a dry glove box.

The IR absorption spectra of binary and oxide-filled electrolyte systems were recorded on a VERTEX 70 Fourier transform spectrometer ("Bruker", Germany) in the range from 4000 cm^{-1} to 370 cm^{-1} with a spectral resolution of at least 0.5 cm^{-1} . The Raman spectra were recorded using a SENTERRA-785 confocal Raman microscope ("Bruker", Germany) with the following technical characteristics: a 532 nm laser (power up to 20 mW); spectral range $50\text{--}1600 \text{ cm}^{-1}$, the microscope lenses $10\times$ and $50\times$, the registration time for one spectrum up to 10 minutes.

A hand-made temperature cell provided high-temperature Raman spectra records in the range from the room temperature up to 200°C .

The IR absorption spectra were recorded by melting the sample and placing it between two plane-parallel high-resistance silicon plates.

The complex bands of experimental spectra were decomposed into components by fitting the calculated curves and the original spectrum using the Levenberg–Marquardt algorithm of absolute error minimization. The shapes of individual bands were fitted by convolution curves of Gaussian and Lorentz functions. The error between the calculated and the experimental curve did not exceed 5%, depending on the signal-to-noise ratio in the original spectrum. All these procedures are implemented in the OPUS 6.0 software package.

XRD diffractograms were taken on a XRD-7000 diffractometer (Shimadzu, Japan). The powder sample was placed in an Anton-Paar TTK-450 temperature chamber, heated up to 80°C under constant vacuum created by a backing vacuum pump, then kept for two hours for additional dehydration, and cooled to ambient temperature.

The record parameters were as follows: standard Bragg–Brentano X-ray focusing, tube voltage 40 kV, current 30 mA, X-ray wavelength $\lambda_{\text{Cu}K\alpha} = 1.5406 \text{ \AA}$, primary nickel filter, scanning $0\text{--}20^\circ$, range $15\text{--}120^\circ$, scanning step size 0.01° , exposure time per one point is 20 s.

The obtained diffractograms were pre-processed using the software implemented in the diffractometer to perform smoothing, background subtraction, account and subtraction of the $\text{Cu}K\alpha_2$ contribution, peak search, account for systematic errors in peak positions. After having identified the phases of the samples, the crystal structures obtained from the initial diffractograms were refined using the Rietveld method. In this case, the diffractograms underwent no additional processing other than background determination. As a result, lattice parameters of each phase were determined with the Rietveld refinement, and the approximate content (C, wt.%) was estimated for each phase, including the determination of the amorphous phase and its approximate content in the samples. The accuracy of determining phase composition by this method was $\pm 3\text{--}5\%$.

The corresponding phases in the samples were determined with the Search Match program from the Shimadzu software package which searches over the ICDD database (International Center for Diffraction Data) PDF-4 + (Powder Diffraction File) containing more than 310,000 articles (diffractograms).

RESULTS AND DISCUSSION

The structures of potassium nitrate and its modifications are well known [12, 13]. Potassium nitrate is orthorhombic *Pnma* (*Pmcn*) at room temperature and atmospheric pressure (phase II) and crystallizes in the aragonite structure with lattice parameters $a = 5.4119 \text{ \AA}$, $b = 9.1567 \text{ \AA}$, $c = 6.4213 \text{ \AA}$ [12]. As the temperature rises to about 403 K, KNO_3 transforms into a disordered phase with calcite structure ($R\bar{3}m$), phase I [13]. When cooled, it transforms from phase I to a new metastable phase III (trigonal $R3m$) at 397 K, and from phase III back to phase II at 383 K. It was discovered recently [14] that phase III is formed not only during the cooling from phase I, but under certain conditions it can be formed and maintained for quite a long time also at room and even lower temperatures.

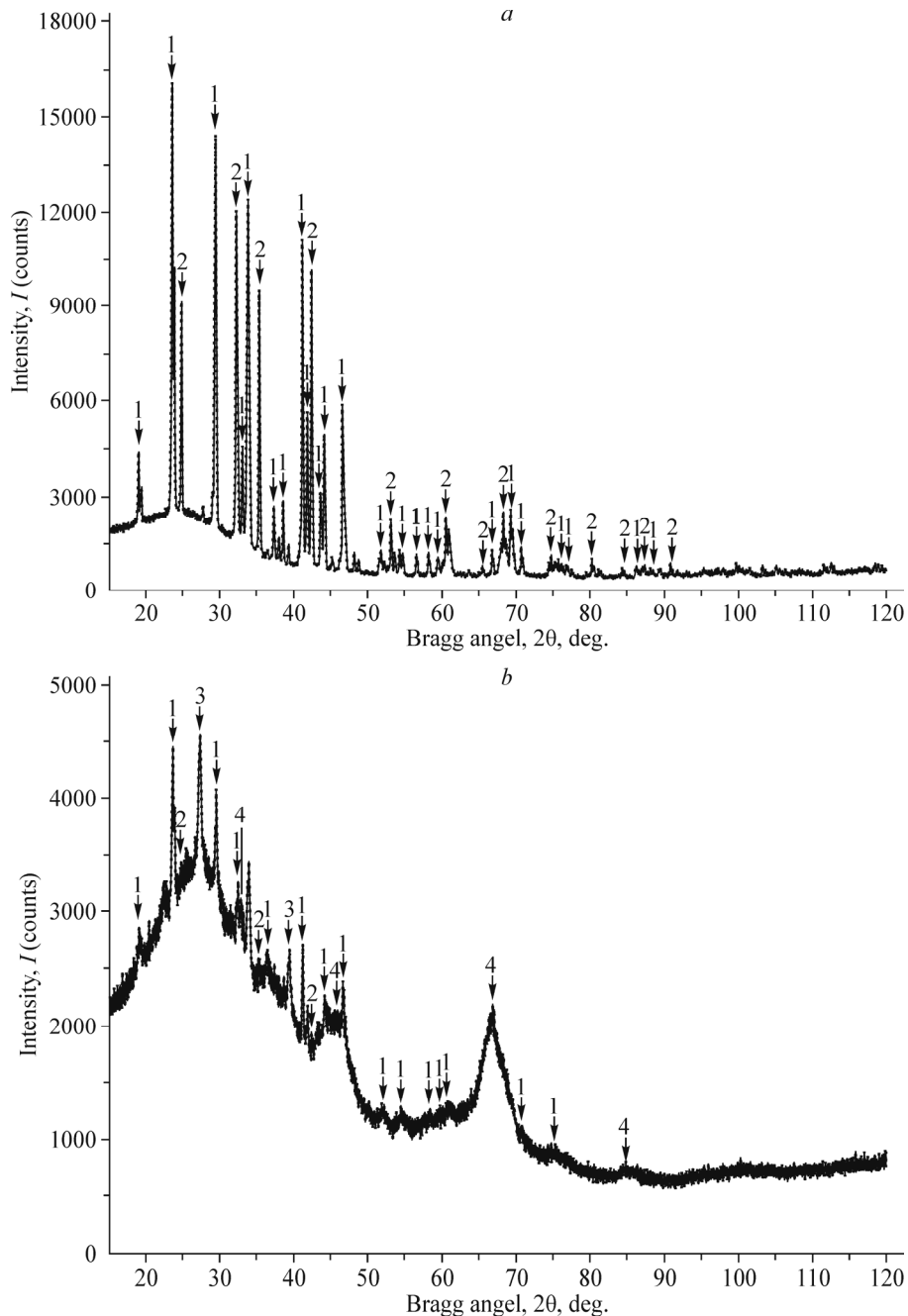


Fig. 1. Diffractogram of $(1-x)\text{Li}_{0.42}\text{K}_{0.58}\text{NO}_3 - x\text{Al}_2\text{O}_3$ for $x = 0$ (a) and $x = 0.7$ (b) at room temperature: KNO_3 , phase II (1); LiNO_3 (2); KNO_3 , phase III (3); Al_2O_3 (2.1/3.2 – Gamma) (4).

Lithium nitrate at room temperature and atmospheric pressure has a hexagonal (rhombohedral) structure, crystallizes in the calcite structural type, $D_{3d}^6-R\bar{3}c$, $Z=6$ (for hexagonal lattice) and $Z=2$ (for rhombohedral lattice) with lattice parameters $a = 4.692 \text{ \AA}$ and $c = 15.215 \text{ \AA}$. This structure is maintained up to the melting point ($T = 253^\circ\text{C}$) [12].

Within the measuring error, the main structural parameters (lattice constants) of LiNO_3 and KNO_3 salts remain almost constant in all samples for all measurement temperatures (Fig. 1). As can be seen from the diffractograms of the composite (Fig. 1b), after the nanosized Al_2O_3 is added, the half width of the peaks of both salts that make up the nanocomposite system increases over the entire range of measured angles to indicate that the size of the grains in the studied powders decreases with the addition of significant amounts of aluminum oxide. Also, the composites with the addition of nanosized alumina demonstrate several small extra peaks in addition to the KNO_3 peaks (phase II, LiNO_3 and Al_2O_3). The search over the ICDD PDF-4+ database testified that these peaks belong to another modification of potassium nitrate, the high-temperature rhombohedral ($R\bar{3}m$) phase III. We previously investigated thermodynamic properties, phase composition, and structure of KNO_3 and its composites with nanosized alumina and reported that these composites contain a high-temperature KNO_3 phase: nanosized and fairly stable phase III [9, 14-16].

This effect is more pronounced for higher Al_2O_3 concentrations. We also calculated weight fractions of each component of the studied composites. The relative percentage of phases (mass fraction C , wt.%) was determined using the Rietveld full-profile refinement. Since the nanosized alumina filler is inert and does not interact with the powder salts when preparing the composites, its initial mass fractions were taken as the constant basis (53.8% for the composition $x = 0.5$ and 73.1% for the composition $x = 0.7$). Thus, Al_2O_3 was used as the inner standard for the quantitative determination of phases after the Rietveld refinement.

The content of crystalline phases was calculated after the conversion to the mass fraction of Al_2O_3 . The residue is an amorphous phase. Since it does not exhibit peaks, its concentration cannot be quantified directly from the X-ray data; therefore, it was calculated indirectly by taking into account the contents of all crystal phases. The Table shows refined

TABLE 1. Refined Lattice Parameters and Approximate Contents (in Mass Fractions C , wt.%) of the Phases (Including the Amorphous Phase) Detected in the Studied Composites, and R -Factors (Divergence Factors) of These Refinements

Sample	$\text{KNO}_3, Pnma$		$\text{KNO}_3, R\bar{3}m$		$\text{LiNO}_3, R-3c$		Aluminium oxide Al_2O_3 –Gamma, $Fm-3m$		Amorphous phase $C, \text{wt.}\%$	$T, {}^\circ\text{C}$ (K)	R_p	R_{wp}	GOOF
	Lattice parameter, \AA , deg.	$C, \text{wt.}\%$	Lattice parameter, \AA , deg.	$C, \text{wt.}\%$	Lattice parameter, \AA , deg.	$C, \text{wt.}\%$	Lattice parameter, \AA , deg.	$C, \text{wt.}\%$					
1	$a = 6.432$ $b = 5.415$ $c = 9.166$ $\alpha = \beta = \gamma = 90$	62	—	—	$a = b = 4.693$ $c = 15.222$ $\alpha = \beta = 90$ $\gamma = 120$	38	—	—	0	25 (298)	6.67	8.49	8,75
2	$a = 6.432$ $b = 5.414$ $c = 9.167$ $\alpha = \beta = \gamma = 90$	21.4	$a = b = 5.427$ $c = 9.133$ $\alpha = \beta = 90$ $\gamma = 120$	2.5	$a = b = 4.696$ $c = 15.236$ $\alpha = \beta = 90$ $\gamma = 120$	5.3	$a = b = c = 7.91$ $\alpha = \beta = \gamma = 90$	53.8	17	25 (298)	4.49	5.89	5,14
3	$a = 6.424$ $b = 5.406$ $c = 9.162$ $\alpha = \beta = \gamma = 90$	5.4	$a = b = 5.456$ $c = 9.053$ $\alpha = \beta = 90$ $\gamma = 120$	4.8	$a = b = 4.692$ $c = 15.221$ $\alpha = \beta = 90$ $\gamma = 120$	0.8	$a = b = c = 7.91$ $\alpha = \beta = \gamma = 90$	73.1	15.9	25 (298)	4.64	6.08	5,41

values of lattice parameters and the approximate phase contents for all composite samples, including amorphous samples. It also presents the values of divergence factors R_p and R_{wp} of the models refined with the Rietveld method.

According to the calculation results, mass fractions of each salt (LiNO_3 and KNO_3) in the total composition of the composite systems decrease with the addition of nanosized Al_2O_3 . The mass fractions of crystal phases of both potassium nitrate (even after partial conversion of KNO_3 from phase II to phase III), and lithium nitrate decrease. This effect is more pronounced for LiNO_3 . For the Al_2O_3 fraction higher than 70 mol.%, the crystalline phase of lithium nitrate is almost not determined.

Fig. 2 shows IR and Raman spectra of the pure binary LiNO_3 – KNO_3 system and of the same system filled with alumina particles.

Nitrate ion in the free state has a D_{3h} point symmetry group, and its vibrations are represented as:

$$\Gamma(D_{3h}) = A'_1 + A''_2 + 2E', \quad (1)$$

with A'_1 and E' being active in the Raman scattering, and A''_2 and E' being active in the IR absorption, where: $v_1(A'_1)$ is a fully symmetric stretching ($\sim 1050 \text{ cm}^{-1}$), $v_2(A''_2)$ is an out-of-plane bending ($\sim 820 \text{ cm}^{-1}$), $v_3(E)$ is a doubly degenerate asymmetric stretching ($\sim 1300 \text{ cm}^{-1}$), $v_4(E)$ is a doubly degenerate bending ($\sim 720 \text{ cm}^{-1}$) [17]. The local symmetry of nitrate ion is D_3 in the LiNO_3 crystal, D_3 in KNO_3 (phase I), and C_s in KNO_3 (phase II). In melts, nitrate anion has either C_{2v} or C_s symmetry. The vibrations A'_1 and E are active both in the Raman spectra and in the IR spectra.

In the IR spectra of the pure mixture at room temperature (Fig. 2b), the bands corresponding to v_2 and v_4 vibrations exhibit a pronounced doublet structure, while the region of the v_1 vibration demonstrates only a barely noticeable weak peak. This suggests that, firstly, the pure binary mixture at room temperature contains two types of nitrate ions with the cationic environment similar to that of individual salts; secondly, the local symmetry of the molecular anion is close to the

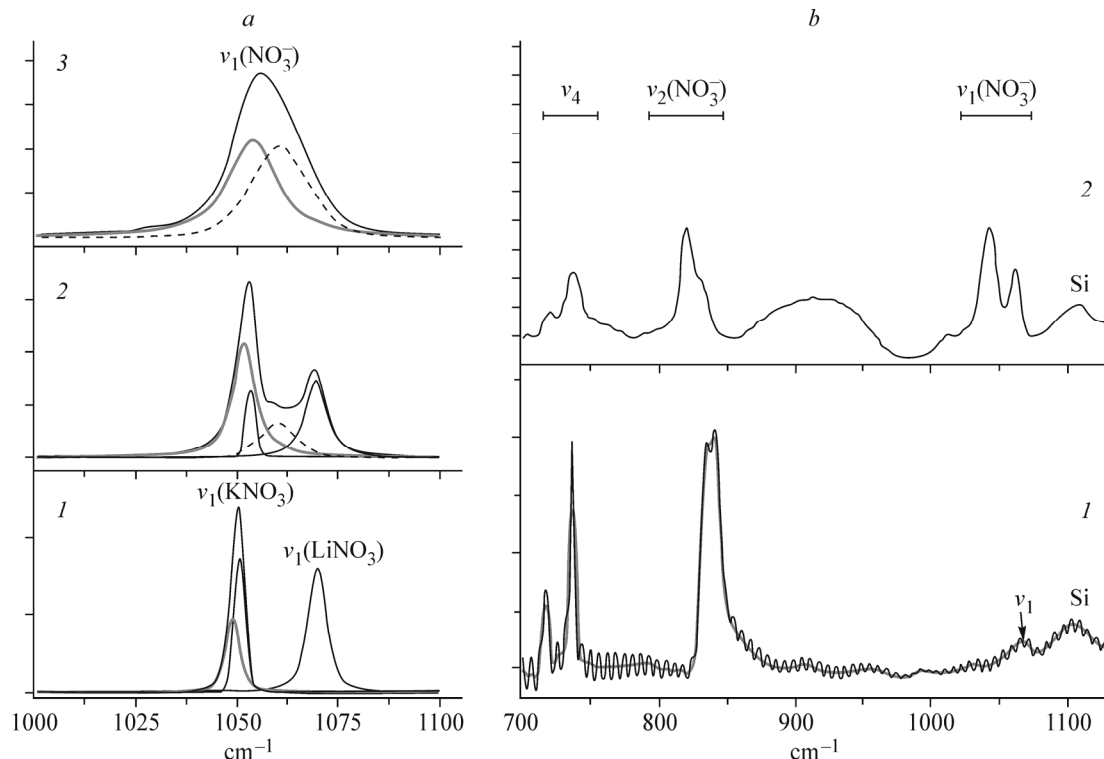


Fig. 2. Vibrational spectra of composites $(1-x)\text{Li}_{0.42}\text{K}_{0.58}\text{NO}_3 - x\text{Al}_2\text{O}_3$: $x = 0$ (1), $x = 0.5$ (2), $x = 0.7$ (3) at room temperature: Raman spectra in the region of fully symmetric stretching $v_1(A'_1)$ of nitrate ion and their decomposition into components (a); IR absorption spectra in the region of vibrations $v_1(A'_1)$, $v_2(A''_2)$, $v_4(E')$ for $x = 0$ and 0.5 (b).

symmetry of isolated NO_3^- . This conclusion is also confirmed by the fact that the Raman spectra of the $\text{LiNO}_3\text{--KNO}_3$ system in the region of the $v_1(A'_1)$ vibration exhibit two clearly separated bands with the peaks appearing close to the lines of the spectra of individual salts (Fig. 2a), i.e. they are a mixture of polycrystals of individual salts. The IR and Raman spectra of the studied system undergo significant changes after the Al_2O_3 powder is added: the contour of the v_4 band in the $\text{LiNO}_3\text{--KNO}_3$ IR spectrum shows a complex shape, which is apparently caused both by the decrease of the NO_3^- local symmetry and the removal of degeneration from the corresponding vibration and, possibly, by a new phase which is formed in the composite and is not present in the pure binary mixture. At the same time, the $v_1(A'_1)$ vibration becomes active in the IR spectra of the $\text{Li,K/NO}_3\text{--Al}_2\text{O}_3$ system for both types of molecular anions.

Let us now consider in more detail the shape of the contours corresponding to fully symmetric vibrations $v_1(A'_1)$ of nitrate ion in the Raman spectra of the alumina-filled system $\text{LiNO}_3\text{--KNO}_3$ from room temperature to the melting point of the salt system. First of all, note that the $v_1(A'_1)$ contour corresponding to NO_3^- vibrations in the KNO_3 sublattice of the pure mixture at room temperature consists of two components that can be assigned to the fluctuations of ordered (frequency 1050 cm^{-1}) and disordered (1047 cm^{-1}) anions in the corresponding sublattice [18], while the same vibration in the Raman spectrum of the LiNO_3 subsystem is a single symmetric line (1070 cm^{-1}) (Fig. 2a). After the alumina powder is added, the Raman spectrum of $\text{Li,K/NO}_3\text{--Al}_2\text{O}_3$ exhibits a complex band in the studied frequency range, which can be decomposed into individual components.

It is noteworthy that the contour of $v_1(A)$ assigned to NO_3^- vibrations in the lithium nitrate sublattice splits into two components with the peaks at $\sim 1060\text{ cm}^{-1}$ and 1070 cm^{-1} , and the proportion of their integral intensities changes in favor of the low-frequency component which increases with the temperature rising up to the melting point of the eutectic (Fig. 3a).

As to the ratio of integral intensities of the components of the bands in the Raman spectra assigned to NO_3^- vibrations in the LiNO_3 and KNO_3 subsystems, it is slightly affected by temperature. In other words, the appearance of an additional component with a peak at $\sim 1060\text{ cm}^{-1}$ in the Raman spectrum of the alumina-filled system is caused, in our opinion, by the appearance of some nitrate ions in the near-surface region at the boundary with alumina particles and by amorphous phase being formed in lithium nitrate [19].

The changes exhibited by the $\text{Li,K/NO}_3\text{--Al}_2\text{O}_3$ spectra with increasing concentration of the inert filler suggest the following conclusions. At alumina concentrations up to ~ 0.5 mole fraction, the changes appear mainly in the crystal lattice of

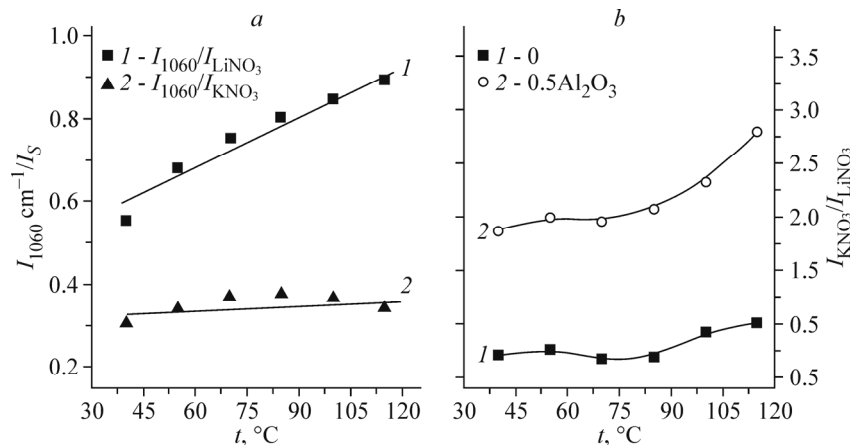


Fig. 3. Temperature dependence of integral ratios of vibrations v_1 ($\sim 1060\text{ cm}^{-1}$) to the intensities of LiNO_3 and KNO_3 components in the composite at $x = 0.5$ (a) and $I_{\text{KNO}_3}/I_{\text{LiNO}_3}$ in the Raman spectra of $(1-x)\text{Li}_{0.42}\text{K}_{0.58}\text{NO}_3 - x\text{Al}_2\text{O}_3$ at $x = 0.5$ (b).

lithium nitrate: the LiNO₃ lattice is subject to amorphization in the near-surface region of the filler particles [19]. At higher filler concentrations, the Raman spectrum in the region of frequency $\nu_1(A)$ is a single wide band (Figs. 2a and 3), which, in our opinion, indicates complete amorphization of both LiNO₃ and KNO₃ subsystems. The conclusions about the structure of the Li,K/NO₃–Al₂O₃ system drawn from purely spectroscopic experiments are confirmed also by XRD data.

CONCLUSIONS

It was shown with Raman and IR absorption spectroscopy methods that the microstructure of the binary salt system Li,K/NO₃ doped with alumina nanopowder undergoes significant changes as compared to the homogeneous binary salt system. The presence of aluminum nano-oxide in the composite results in the amorphous phase being formed in the system. According to the obtained powder XRD and spectroscopic data, the amorphization caused by low concentrations of Al₂O₃ (below 0.5) proceeds mainly due to the destruction of the lithium nitrate crystal lattice.

ACKNOWLEDGMENTS

The work was performed on the equipment of the Analytical Center of Joint Usage, Dagestan Scientific Center, Russian Academy of Sciences.

CONFLICT OF INTERESTS

The authors declare that they have no conflict of interests.

REFERENCES

1. N. F. Uvarov, E. F. Hairetdinov, and I. V. Skobelev. *Solid State Ionics*, **1996**, 86-88, 577–580.
2. N. F. Uvarov, A. S. Ulihin, and Yu. G. Mateyshina. *Chem. Sustainable Dev.* [In Russian], **2012**, 20, 95.
3. M. V. Madhava Rao, S. Narendra Reddy, A. Sadananda Chary, and K. Shahi. *Physica B: Condensed Matter*, **2005**, 364, 306.
4. A. R. Aliev, I. R. Akhmedov, M. G. Kakagasanov, Z. A. Aliev, M. M. Gafurov, K. Sh. Rabadanov, and A. M. Amirov. *Phys. Solid State* [In Russian], **2017**, 59(4), 752-757.
5. J. Maier. *J. Electrochem. Soc.*, **1987**, 134, 1524.
6. U. W. Li, S. Zhu, D. Wang et al. Extended Abstract: International Conference on Solid State Ionics. Singapore, **1995**, 105.
7. M. M. Gafurov, A. R. Aliev, M. B. Ataev, and K. Sh. Rabadanov. *Spectrochim. Acta Part A*, **2013**, 114, 563.
8. M. M. Gafurov, K. Sh. Rabadanov, M. B. Ataev, A. M. Amirov, Z. Yu. Kubataev, and A. R. Aliev. *J. Struct. Chem.* **2015**, 56(3), 428-435.
9. M. B. Ataev, M. M. Gafurov, K. Sh. Rabadanov, A. M. Amirov, and R. M. Emirov. *Phys. Solid State*. **2016**, 58(12), 2423-2426.
10. A. M. Amirov, M. M. Gafurov, and S. I. Suleymanov. *J. Therm. Anal. Calorim.*, **2017**, 1–5.
11. N. F. Uvarov. Composite solid electrolytes. Novosibirsk: Izd-vo SO RAN, **2008**.
12. J. K. Nimmo and B. W. Lucas. *J. Phys. C: Solid State Phys.* **1973**, 6, 201.
13. J. K. Nimmo and B. W. Lucas. *Acta Crystallogr.*, **1976**, B32, 1968.
14. R. Poprawski, E. Rysiakiewicz-Pasek, A. Sieradzki, A. Man, J. Polanska. *J. Non-Cryst. Solids*, **2007**, 353, 4457.
15. E. J. Freney, L. A. J. Garvie, T. L. Groy, and P. R. Busecka. *Acta Crystallogr.*, **2009**, B65, 659.
16. X. Wu, F. R. Fronczek, and L. G. Butler. *Inorg. Chem.*, **1994**, 33, 1363.
17. K. Nakamoto. Infrared and Raman Spectra of Inorganic and Coordination Compounds. M: Mir, **1991**, 536.
18. M. Y. Brooker. *J. Phys. Chem. Solids*, **1978**, 39, 657.
19. M. M. Gafurov, K. Sh. Rabadanov, M. B. Ataev, A. M. Amirov, Z. Y. Kubataev, and M. G. Kakagasanov. *Phys. Solid State* [In Russian]. **2015**, 57 (10), 2066-2072.